NEUROSCIENCE

Dendritic axon origin enables information gating by perisomatic inhibition in pyramidal neurons

Alexander Hodapp[1]†, Martin E. Kaiser[1]†, Christian Thome[1,2,3], Lingjun Ding[4,5,6], Andrei Rozov[1,7,8], Matthias Klumpp[1], Nikolas Stevens[1], Moritz Stingl[1], Tina Sackmann[1], Nadja Lehmann[9], Andreas Draguhn[1], Andrea Burgalossi[4,5], Maren Engelhardt[2,9], Martin Both[1]*

Information processing in neuronal networks involves the recruitment of selected neurons into coordinated spatiotemporal activity patterns. This sparse activation results from widespread synaptic inhibition in conjunction with neuron-specific synaptic excitation. We report the selective recruitment of hippocampal pyramidal cells into patterned network activity. During ripple oscillations in awake mice, spiking is much more likely in cells in which the axon originates from a basal dendrite rather than from the soma. High-resolution recordings in vitro and computer modeling indicate that these spikes are elicited by synaptic input to the axon-carrying dendrite and thus escape perisomatic inhibition. Pyramidal cells with somatic axon origin can be activated during ripple oscillations by blocking their somatic inhibition. The recruitment of neurons into active ensembles is thus determined by axonal morphological features.

A hallmark of neuronal network activity is the selective recruitment of neurons into active ensembles, which form transiently stable patterns of activity (*1*–*3*). In the mammalian hippocampus, the repetitive activation of such neuronal ensembles during ripple (~200 Hz) oscillations supports the consolidation of spatial and declarative memories (*4*, *5*). A central question is how individual neurons are selected for participation in these patterns of coactivity. The activation of specific neurons has been suggested to result from the convergence and use-dependent plasticity of excitatory synapses (*6*, *7*). By contrast, the global, strong perisomatic inhibition would provide a common, unspecific gain control mechanism for all local neurons and an oscillating temporal scaffold for the embedded spatiotemporal activity patterns (*8*). Recent work has revealed a marked morphological and functional heterogeneity among principal cells in cortical networks (*9*–*12*), including the nonsomatic (dendritic) origin of axons in a subset of pyramidal cells (Fig. 1, A to C) (*13*, *14*). The differential recruitment of individual neurons could be determined by the morphological feature of axon onset. We studied this possibility in hippocampal ripple oscillations, which activate specific neuronal ensembles and recruit pronounced perisomatic inhibition (*15*, *16*).

We recorded juxtacellular activity from single neurons in the CA1 region of awake, head-fixed mice together with local field potentials representing the overall network state (Fig. 1, D and E). In CA1, ~50% of pyramidal cells have an axon originating from a basal dendrite (fig. S1) (*13*), opening the possibility of a functional distinction between axon-carrying dendrite cells (AcD cells) and canonical non-AcD cells. This distinction is further supported by a bimodal distribution of the distance between soma and axon initial segment (fig. S1C). Cells were filled with biocytin, reconstructed ex vivo, and classified into two groups with respect to the site of axon origin (Fig. 1, B and C, and figs. S1 to S3). During in vivo recordings, the firing probability of AcD cells during ripples was ~4.5-fold higher than for non-AcD cells, and the firing frequency during ripples was ~2.5-fold higher (Fig. 1, F and G, and table S1). By contrast, there was no difference in firing frequency outside of ripples (Fig. 1H and table S1). A more detailed analysis of field potentials revealed a difference in the power of spike-accompanied ripples, with larger power for AcD than non-AcD cells. AcD cells therefore fire spikes during cycles with particularly strong inhibition, in contrast to non-AcD cells (Fig. 1I and table S1) (*15, 16*).

We hypothesized that the preferred ripple-associated firing of AcD cells is caused by their morphology: Excitatory inputs to the axon-carrying basal dendrite escape perisomatic inhibition and allow action potential (AP) generation even during pronounced activation of γ-aminobutyric acid (GABA)–ergic interneurons. We tested this mechanism in acute hippocampal slices, which allowed us to study cell-network coupling under well-controllable conditions (*17*). The preferential activation of AcD cells during ripples was maintained in this preparation (Fig. 2, A and B, and table S2). First, we assessed whether AcD and non-AcD cells receive different synaptic input during ripples. Subthreshold inhibitory and excitatory postsynaptic potentials were recorded at different membrane potentials and revealed similar inhibition-excitation conductance ratios (I/E) (*18*) for both cell types. Likewise, the inhibitory and excitatory current ratio was not different (Fig. 2C and tables S2 and S3). There was no difference in the relative timing of inhibitory and excitatory events (fig. S4, A and B, and tables S2 and S3). A direct analysis of perisomatic inhibition by paired recordings from fast-spiking parvalbumin-positive inhibitory interneurons and pyramidal cells confirmed identical coupling probability and strength for AcD and non-AcD cells, respectively (Fig. 2D; fig. S4, C to E; and tables S4 and S5). Is the proposed privileged role of the axon-carrying basal dendrite reflected in peculiar morphological features? Both AcD and non-AcD cells had a similar number of basal dendrites (median = 3) (Fig. 2, E and F, and tables S3 to S5) and no differences in branching pattern, total dendritic length, and spine density (Fig. 2, G and H, and fig. S5). However, the AcD was longer than basal dendrites of non-AcD cells and made up for ~35% of basal dendritic length (~12% of total dendritic length in our reconstructed neurons) (Fig. 2I; supplementary materials, materials and methods; fig. S5C; and tables S3 to S5), which indicates a significant weight of synaptic input to this particular dendrite. Nevertheless, synaptic inhibition, I/E ratio, and dendritic arborization were largely similar between both cell types. Thus, factors other than synaptic input seem to determine the preferential firing of AcD cells. This hypothesis is further supported by the more negative threshold of ripple-associated APs in AcD cells, which is indicative of a noncanonical site of AP initiation (Fig. 2K and table S2) (*17*).

To assess the impact of axon origin on firing probability and threshold under different conditions of synaptic input, we used a detailed multicompartment cellular computer model (Fig. 3). Cells consisted of a soma and three dendrites with axon origin at the soma (non-AcD) or a basal dendrite (AcD), respectively (Fig. 3A). First, we modeled transient excitatory input to the AcD together with transient perisomatic inhibition, with typical postsynaptic kinetics observed during ripples. AcD cells fired APs more readily than did non-AcD cells and generated AP waveforms indicative of distal AP initiation (Fig. 3A). A systematic variation of inhibitory and excitatory input strength revealed a much broader variety of synaptic input combinations that triggered APs in AcD compared with non-AcD cells

[1]Institute of Physiology and Pathophysiology, Medical Faculty, Heidelberg University, Heidelberg, Germany. [2]Institute of Anatomy and Cell Biology, Medical Faculty, Johannes Kepler University, Linz, Austria. [3]Institute for Stem Cell Biology and Regenerative Medicine, Stanford University, Stanford, CA, USA. [4]Institute of Neurobiology, University of Tübingen, Tübingen, Germany. [5]Werner-Reichardt Centre for Integrative Neuroscience, Tübingen, Germany. [6]Graduate Training Centre of Neuroscience, IMPRS, Tübingen, Germany. [7]Federal Center of Brain Research and Neurotechnologies, Moscow, Russian Federation. [8]OpenLab of Neurobiology, Kazan Federal University, Kazan, Russian Federation. [9]Institute of Neuroanatomy, Mannheim Center for Translational Neuroscience (MCTN), Medical Faculty Mannheim, Heidelberg University, Heidelberg, Germany.
*Corresponding author. Email: mboth@physiologie.uni-heidelberg.de
†These authors contributed equally to this work.

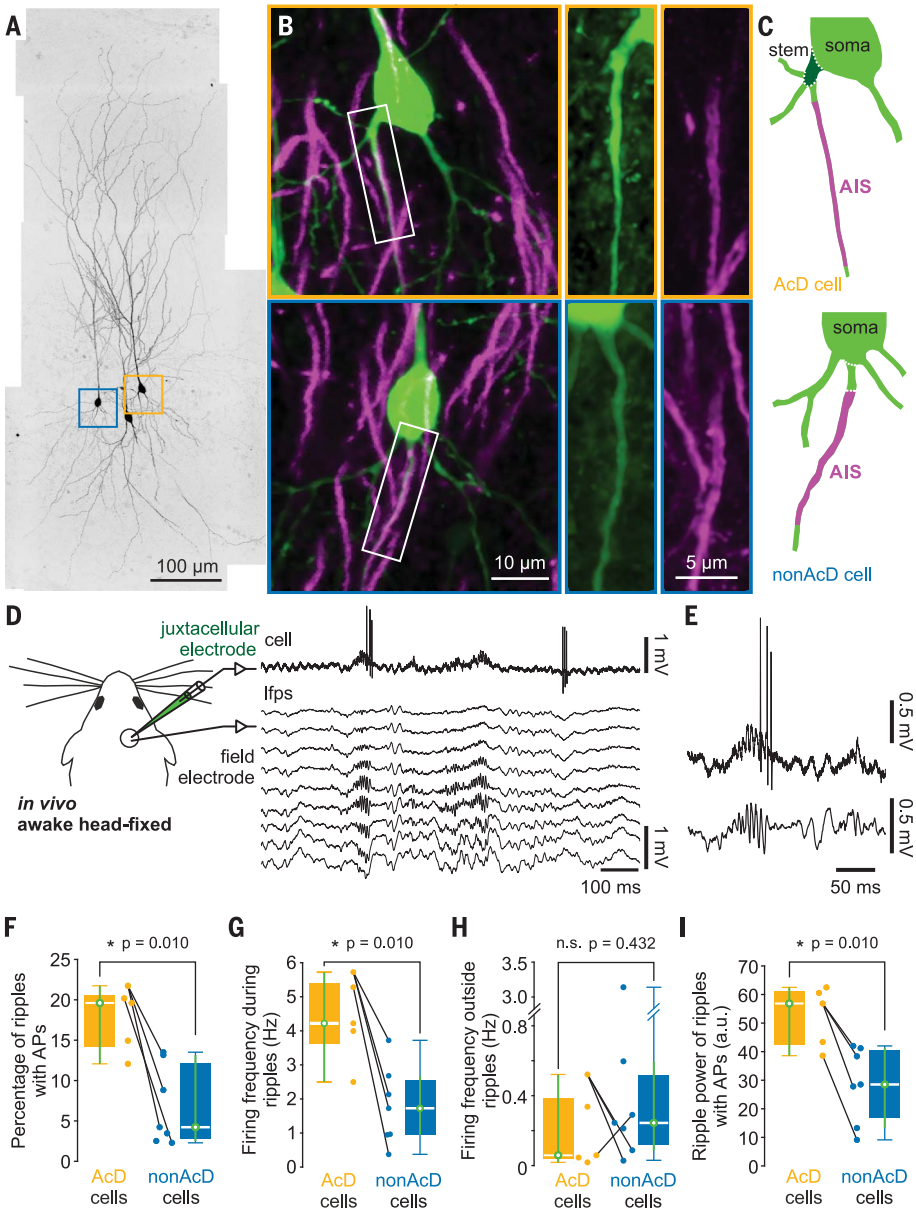

Fig. 1. Preferential recruitment of AcD cells during ripples in vivo. (**A** to **C**) Distinction between AcD and non-AcD cells. (A) Reconstruction of biocytin-filled pyramidal cells (left and right) together with a fast-spiking interneuron (middle) (Fig. 2 and fig. S4). (B) Soma-near region of the AcD (top) and non-AcD (bottom) cell. Cell is in green, axon initial segment (AIS) is in magenta, and the overlay is outlined in white. (C) Schematic representation showing the dendritic origin of the AcD cell. Details are available in figs. S1 and S2. (**D**) Single hippocampal CA1 pyramidal neurons were recorded juxtacellularly in awake, head-fixed mice. Simultaneously, local field potentials (lfps) were recorded with a 16-channel silicon probe. Ripples were identified by their characteristic frequency of 140 to 200 Hz. (**E**) Magnification of a representative ripple event from recording in (D). (**F**) Percentage of ripples with APs was larger for AcD cells than for non-AcD cells. (**G**) Similarly, AcD cells had a higher firing frequency during ripples than that of non-AcD cells. (**H**) Firing frequency outside of ripples was not different. n.s., not significant. (**I**) Mean power of ripples with APs was larger for AcD cells than for non-AcD cells. Cells recorded in the same animal are connected by black lines (five AcD cells from four animals and seven non-AcD cells from four animals). a.u., arbitrary unit.

(Fig. 3B). Firing thresholds were decidedly more negative for AcD cells, which is consistent with our experimental findings (Fig. 4C). Recording electrodes are typically located in the soma, yielding different apparent I/E conductance ratios compared with the site of origin of the synaptic conductances. Such apparent (somatically recorded) conductance ratios in a model cell are shown in Fig. 3B, bottom. Strong increases in local (dendritic) AMPA conductance can go along with small changes in apparent I/E ratio. Thus, APs in AcD cells may be caused by particularly strong excitation of the AcD, whereas somatically recorded I/E ratios appear similar for AcD and non-AcD cells. This mechanism implies that in the presence of perisomatic inhibition, excitatory input to the AcD becomes more efficient with increasing distance between axon and soma. This was confirmed in model calculations: The difference in excitability by input to the AcD versus non-AcD branch was increased by increasing axon-to-soma distance as well as by increasing perisomatic inhibition (Fig. 3C). The increased AP propensity of AcDs was markedly present even at short axon distances <5 µm, covering the empirical distribution of axon onsets (fig. S1, C and D). Thus, the model supports our hypothesis and emphasizes the privileged function of the AcD for participation in network activity.

The causal relationship between axon origin, perisomatic inhibition, and firing propensity predicts that functional differences between AcD and non-AcD cells should be diminished when perisomatic inhibition is reduced. We tested this by blocking GABA type A ($GABA_A$) receptors in individual pyramidal cells by means of picrotoxin loading through the intracellular pipette, which leaves the network-level I/E balance unaltered (Fig. 4, A and B). This procedure resulted in a strongly reduced intracellular I/E conduction ratio and increased firing probability (Fig. 4C and table S2). Under these conditions, non-AcD cells readily fired APs during ripples, in contrast to recordings with intact inhibition. Likewise, the apparent somatic AP threshold was shifted to more positive values, as predicted by our model (Fig. 4C, right, and table S2). Because of their higher firing propensity in this paradigm, the ripple-associated firing of non-AcD cells allowed for a correlation analysis between I/E ratio and firing probability. The result supports our proposed mechanism: Non-AcD cells showed a highly significant correlation, with lower I/E ratios favoring firing during ripples, whereas

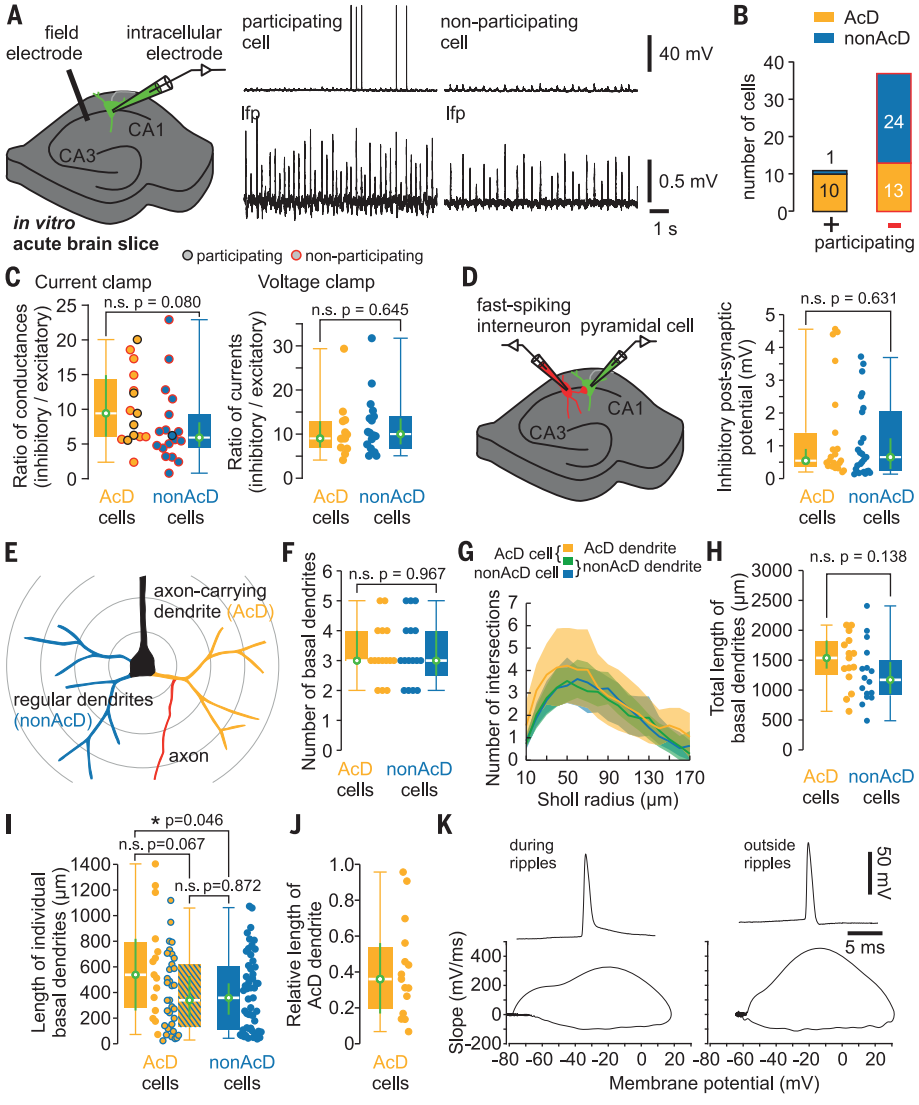

Fig. 2. AcD and non-AcD cells receive similar synaptic input and have similar dendritic morphology. (**A**) Single hippocampal CA1 pyramidal neurons were recorded with sharp electrodes in acute brain slices from mice. Simultaneously, the lfp was recorded with a single field electrode. Ripple oscillations occurred spontaneously and could be well detected by the prominent positive sharp wave (bottom right). Neurons were classified into participating cells (firing spikes during ripples) and nonparticipating cells. (**B**) Similar to in vivo ripples, AcD cells have a higher propensity to fire APs during ripples than that of non-AcD cells (P = 0.002, Fisher's exact test). (**C**) Subthreshold excitatory and inhibitory synaptic events during ripples. Ratios of conductance changes (from current clamp experiments) and currents (from voltage clamp experiments) are similar in AcD and non-AcD cells. (**D**) Paired whole-cell recordings from presynaptic parvalbumin-positive fast-spiking inhibitory interneurons and postsynaptic CA1 pyramidal neurons. Connection probability (47.8% for AcD cells and 53.2% for non-AcD cells; P = 0.680) and synaptic strength were not different between the two groups (22 connected of 46 recorded AcD cells versus 25 connected of 47 recorded non-AcD cells). In these experiments, high-chloride intracellular solution was used to artificially render inhibitory postsynaptic potentials depolarizing at resting membrane potential for more accurate quantification. (**E** to **J**) Morphology of basal dendrites was analyzed and compared between AcD and non-AcD cells. (F) The number of basal dendrites is not different between the two groups. (G) Sholl analysis reveals a tendency to higher complexity of AcDs compared with canonical dendrites in both AcD and non-AcD cells. (H) Total length of basal dendrites is not different between AcD and non-AcD cells. (I) AcDs are longer than canonical dendrites from non-AcD cells. (J) AcDs compose 36% of the total length of basal dendrites in AcD cells. Data were quantified from 15 AcD cells versus 16 non-AcD cells. (**K**) APs occurring during ripples have a more negative voltage threshold than APs occurring outside ripples. Phase plots show that APs recorded at the soma during ripples consist of two distinct phases during the upstroke, indicating an electrically distant origin of the AP.

AcD cell firing was much less dependent on the I/E ratio (Fig. 4D).

Together, these findings reveal a mechanism for differential recruitment of pyramidal neurons into network activity, depending on their axon origin. AcD cells retain the ability to fire APs even in situations in which firing of canonical (non-AcD) pyramidal cells is largely prohibited by GABAergic inhibition (Fig. 4E). In such network states, activation of AcD cells is largely confined to excitatory inputs at the AcD. The AcD contains ~1/3 of all spines at basal dendrites and makes up a relevant part of the entire dendritic tree (Fig. 2I and fig. S5), likely receiving notable excitatory input. The privileged function of this dendrite allows for state-dependent switches of the functional connectivity of the network: During phases of strong perisomatic inhibition, excitatory inputs are most efficient at the AcD, whereas during less pronounced perisomatic inhibition, inputs to all dendrites contribute more equally (Fig. 4E). This morpho-functional mechanism explains how specific cells are preferentially activated during ripples in hippocampal networks (*19*–*21*). Thus, the site of axon origin in combination with perisomatic inhibition defines the group of potentially active neurons (Fig. 4F), whereas the individual members of active ensembles are likely selected by additional mechanisms, including the strength and plasticity of excitatory synaptic inputs (*22*). According to our model, a substantial portion of this input must arrive at the axon-carrying basal dendrite, which expresses supralinear signal integration (*13*) and may, therefore, contribute to the temporal precision of firing during high-frequency ripple oscillations (*23*). Axon distance from the soma is a continuous parameter (fig. S1, C and D), and hence, the degree of functional coupling to ripples may vary between cells. However, even our simplified, categorial classification shows large differences of AcD versus non-AcD cell recruitment (Figs. 1 and 2).

The selective activation of neurons is fundamental for information processing and memory formation in cortical networks (*1*–*3*, *24*). Although the underlying mechanisms are largely unresolved, most models emphasize differences in excitatory synaptic activation (*6*, *7*, *9*–*11*, *19*–*21*). Recent evidence shows that neurons that underwent learning-related plasticity subsequently display increased synaptic excitation and participation in ripple oscillations (*22*). Our data provide an additional, complementary mechanism for preselection of activatable neurons: We propose that the location of the axon is a key determinant of asymmetric recruitment in oscillating network states. Excitatory inputs on AcDs evade perisomatic inhibition, so that AcD cells are clearly more prone to participate in ripple oscillations. This discovery helps to explain how the

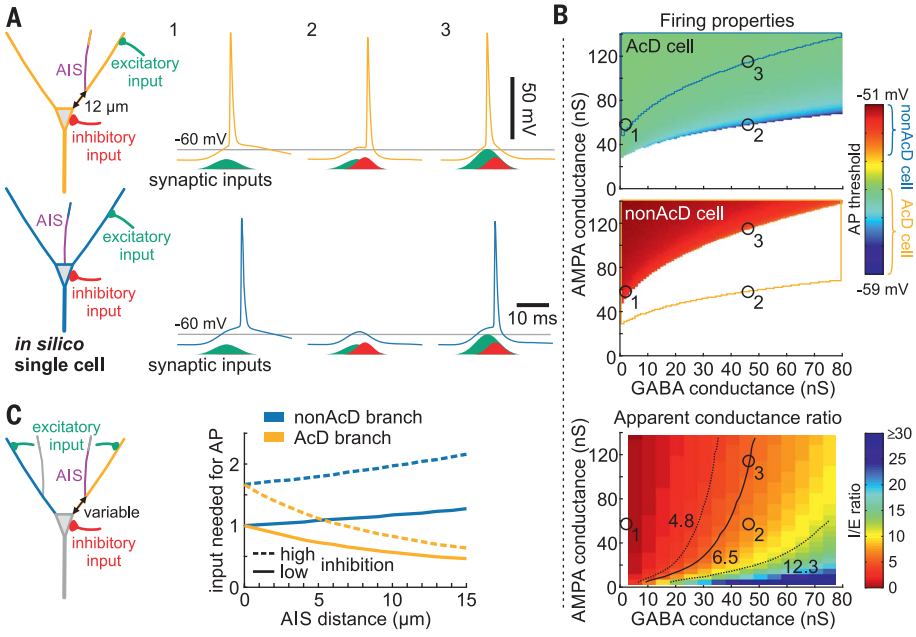

Fig. 3. Single-cell multicompartment computer modeling predicts the observed differences in firing behavior between AcD and non-AcD cells. (**A**) (Left) Schematics of an AcD cell with an axon origin at 12 µm from (top) the soma and (bottom) a non-AcD cell. (Right) Three different conditions of phasic synaptic inputs leading to different propensities of AP generation and AP thresholds. (**B**) Firing and AP threshold for a broad range of inhibitory (*x* axis) and excitatory (*y* axis) conductance changes. Colors indicate the firing threshold. White areas indicate that no AP was generated. The three different conditions shown in (A) are marked by circles. (Top) Firing of the model AcD cell. The blue line indicates limits of AP generation for the non-AcD cell. (Middle) Firing and AP threshold of the model non-AcD cell. The yellow line indicates the limits of AP generation for the AcD cell. (Bottom) Apparent I/E ratio as assessed from a simulated somatic recording. The 25th, 50th, and 75th percentile of conductance ratios recorded in single neurons in vitro (Figs. 2C and 4C) are indicated with black lines (numbers show the according I/E ratio). (**C**) In AcD cells, AcD branch has a higher propensity to elicit APs than do non-AcDs. This difference increases with axon distance (*x* axis) and with higher I/E ratio (dotted versus straight lines).

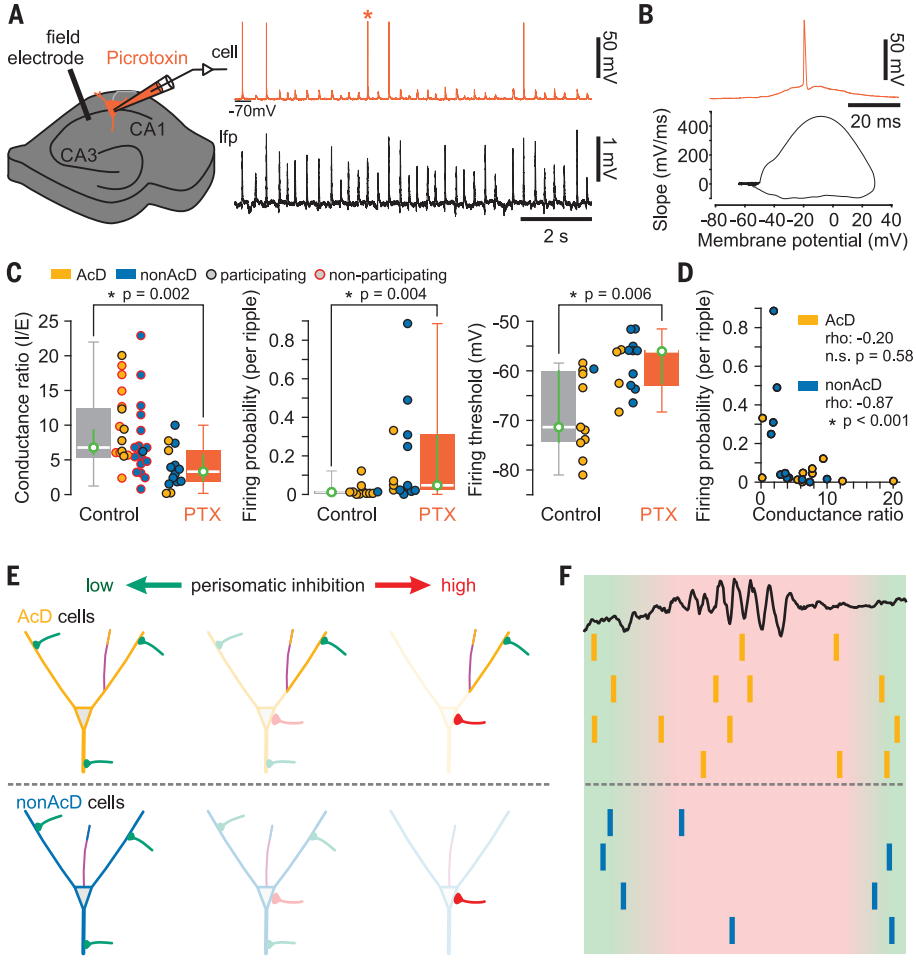

Fig. 4. Differential gating of information processing by perisomatic inhibition in AcD and non-AcD cells. (**A**) GABAergic transmission to the recorded cell was blocked by adding picrotoxin (1 mM) to the internal electrode solution, leaving global network oscillations unchanged. This enabled the recorded non-AcD cell to fire APs during ripples [classified as participating cells (Fig. 4C)]. (**B**) Phase plot of the AP marked by an asterisk in (A). There is similarity to Fig. 2K, right, which is indicative of a canonical location of AP generation. (**C**) Reducing perisomatic inhibition diminishes differences in firing characteristics of AcD and non-AcD cells during ripples. (Left) I/E ratio is strongly reduced by intracellular picrotoxin. (Middle) Picrotoxin-filled cells, including non-AcD cells, increase their firing probability during ripples. (Right) Additionally, firing thresholds shift to more positive values, which is typical for canonical AP generation. PTX, picrotoxin. (**D**) Firing probability is negatively correlated with I/E conductance ratio in non-AcD cells but not in AcD cells. (**E**) Schematic representation of the different excitability of AcD and non-AcD cells, respectively. Perisomatic inhibition increases from left to right. (Bottom) In non-AcD cells, AP generation is globally suppressed under perisomatic inhibition. In AcD cells, however, AP generation is still possible upon excitatory inputs at the AcD. (**F**) AcD cells maintain the possibility of firing APs even in situations of pronounced inhibition, such as ripple oscillations.

activation of selected pyramidal cells can be reconciled with the strong and global perisomatic inhibition during network oscillations. It will be important to study whether the site of axon origin undergoes activity-dependent structural plasticity, similar to the established homeostatic remodeling of the axon initial segment that regulates cellular excitability (*25*–*29*). Likewise, it remains to be shown whether AcDs receive excitatory input from specific upstream areas, especially during network states with strong inhibition. Given the abundance of similar axon morphologies in other cortical and subcortical areas of the vertebrate brain (*14*, *30*–*34*), it may well be that the selection of active neurons by their axon origin is a more widespread principle.

REFERENCES AND NOTES

1. B. M. Sweis, W. Mau, S. Rabinowitz, D. J. Cai, *Curr. Opin. Neurobiol.* **67**, 199–206 (2021).
2. G. Dragoi, *Curr. Opin. Neurobiol.* **64**, 111–118 (2020).
3. L. Carrillo-Reid, R. Yuste, *Curr. Opin. Neurobiol.* **64**, 89–95 (2020).
4. G. Girardeau, K. Benchenane, S. I. Wiener, G. Buzsáki, M. B. Zugaro, *Nat. Neurosci.* **12**, 1222–1223 (2009).
5. A. Fernández-Ruiz *et al*., *Science* **364**, 1082–1086 (2019).
6. G. Buzsáki, *Neuron* **68**, 362–385 (2010).
7. D. O. Hebb, *The Organization of Behavior—A Neuropsychological Theory* (Psychology Press, 1949).
8. G. Buzsáki, D. Tingley, *Trends Cogn. Sci.* **22**, 853–869 (2018).
9. I. Soltesz, A. Losonczy, *Nat. Neurosci.* **21**, 484–493 (2018).
10. F. Sharif, B. Tayebi, G. Buzsáki, S. Royer, A. Fernandez-Ruiz, *Neuron* **109**, 363–376.e6 (2021).
11. M. Valero *et al*., *Nat. Neurosci.* **18**, 1281–1290 (2015).
12. L. Ding *et al*., *eLife* **11**, e71720 (2022).
13. C. Thome *et al*., *Neuron* **83**, 1418–1430 (2014).
14. P. Wahle *et al*., *eLife* **11**, e76101 (2022).
15. J. Gan, S. M. Weng, A. J. Pernía-Andrade, J. Csicsvari, P. Jonas, *Neuron* **93**, 308–314 (2017).
16. D. F. English *et al*., *J. Neurosci.* **34**, 16509–16517 (2014).
17. F. Bähner *et al*., *Proc. Natl. Acad. Sci. U.S.A.* **108**, E607–E616 (2011).
18. L. J. Borg-Graham, C. Monier, Y. Frégnac, *Nature* **393**, 369–373 (1998).
19. J. Epsztein, M. Brecht, A. K. Lee, *Neuron* **70**, 109–120 (2011).
20. J. S. Lee, J. J. Briguglio, J. D. Cohen, S. Romani, A. K. Lee, *Cell* **183**, 620–635.e22 (2020).
21. K. Z. Tanaka *et al*., *Science* **361**, 392–397 (2018).
22. M. Mizunuma *et al*., *Nat. Neurosci.* **17**, 503–505 (2014).
23. S. Jahnke, M. Timme, R. M. Memmesheimer, *J. Neurosci.* **35**, 16236–16258 (2015).
24. J. Wolfe, A. R. Houweling, M. Brecht, *Curr. Opin. Neurobiol.* **20**, 306–312 (2010).
25. N. Jamann *et al*., *Nat. Commun.* **12**, 23 (2021).
26. H. Kuba, Y. Oichi, H. Ohmori, *Nature* **465**, 1075–1078 (2010).
27. M. S. Grubb, J. Burrone, *Nature* **465**, 1070–1074 (2010).
28. W. Wefelmeyer, D. Cattaert, J. Burrone, *Proc. Natl. Acad. Sci. U.S.A.* **112**, 9757–9762 (2015).
29. K. Martinello *et al*., *Neuron* **85**, 346–363 (2015).
30. M. H. Kole, R. Brette, *Curr. Opin. Neurobiol.* **51**, 52–59 (2018).
31. M. S. Hamada, S. Goethals, S. I. de Vries, R. Brette, M. H. Kole, *Proc. Natl. Acad. Sci. U.S.A.* **113**, 14841–14846 (2016).
32. L. C. Triarhou, *Front. Neuroanat.* **8**, 133 (2014).
33. F. Höfflin *et al*., *Front. Cell. Neurosci.* **11**, 332 (2017).
34. M. Häusser, G. Stuart, C. Racca, B. Sakmann, *Neuron* **15**, 637–647 (1995).

ACKNOWLEDGMENTS

We thank L. Menendez de la Prida, M. Valero, J. Epsztein, C. Bernard, and T. Künsting for insightful discussions and comments and N. Zuber, Y. Yanovsky, P. Geschwill, B. Throm, and J. M. Janssen for excellent technical assistance. We acknowledge the Nikon Imaging Center at Heidelberg University and Nikon for access to laser scanning confocal microscopy (A1 and AXR). **Funding:** This work was supported by the German Research Foundation (grant SFB1134, projects A01 and A03, DFG BO 3512/2-1, DFG EN 1240/2-1, DFG BU 3126/2-1, and DFG WBP Fellowship PN 458054460). **Author contributions:** M.B., M.E., A.B., and A.D. conceived of and designed the experiments; A.H., M.E.K., L.D., M.K., A.R., M.S., and M.B. performed experiments; A.H., M.E.K., C.T., M.E., A.R., N.S., N.L., T.S., and M.B. analyzed the data; and M.B. and A.D. wrote the original manuscript. All authors revised and edited the manuscript. **Competing interests:** The authors declare that they have no competing interests. **Data and materials availability:** The data and analysis scripts that support the findings of this study are publicly available at https://doi.org/10.11588/data/JWLFFZ.

SUPPLEMENTARY MATERIALS

science.org/doi/10.1126/science.abj1861
Materials and Methods
Figs. S1 to S5
Tables S1 to S6
References (*35*–*55*)
MDAR Reproducibility Checklist

View/request a protocol for this paper from *Bio-protocol*.

Submitted 28 April 2021; resubmitted 3 June 2022
Accepted 19 August 2022
10.1126/science.abj1861